Photoemission study of Fermi surfaces of pseudomorphic Co, Ni, and Co_xNi_{1-x} films on Cu(100)

Michael Hochstrasser, Nat Gilman, and Roy F. Willis
Physics Department, Pennsylvania State University, 104 Davey Laboratory, University Park, Pennsylvania 16802

Frank O. Schumann and James G. Tobin
Lawrence Livermore National Laboratory, Livermore, 7000 East Avenue, Livermore, California 94550

Eli Rotenberg
Lawrence Berkeley National Laboratory, Advanced Light Source, 1 Cyclotron Road, Berkeley, California 94720
(Received 22 July 1999)

The *k*-space electronic structure of Co_xNi_{1-x} alloy films epitaxially grown on Cu(100) has been investigated with changing stoichiometry in angle-resolved photoemission, and is compared to the electronic structure of fcc films of Co and Ni, and single-crystalline Cu. We have monitored changes in the Fermi surface with changing stoichiometry and changing magnetic behavior. The measurements show that the *sp* band is a prominent feature of the Fermi surface throughout *k* space for all of the alloys and the magnetic $3d$ pseudomorphic fcc films. A band-structure calculation of Ni allows us to identify *d*-hole pockets which increase in size with changing stoichiometry. Minority spin states highlight specific regions of *k* space associated with key spanning vectors that determine the oscillatory exchange coupling, which underpins the giant magnetoresistance effect in heterostructures. [S0163-1829(99)03948-X]

I. INTRODUCTION

The exchange coupling between ferromagnetic layers across a nonmagnetic interlayer has attracted much attention and has been observed in numerous systems.[1] The magnetization vectors *M* oscillate between parallel and antiparallel ordering between the magnetic layers, depending on the thickness of the intervening nonmagnetic metallic interlayer.[2] This oscillatory behavior of the interlayer exchange coupling can be understood in terms of Ruderman-Kittel-Kasuya-Yosida (RKKY) oscillations in the electronic density, which predicts the different oscillation periods originating from extremal spanning vectors of the Fermi surface of the spacer material.[3–5] In the case of copper spacer heterostructures, spanning vectors have been identified with particular wave vectors spanning particular regions of the ''dogbone'' structure of the Fermi surface formed by the (*sp*) states. A ''long period'' oscillation is observed, corresponding to a wave vector spanning the midpoints of the ''dogbone.''[6] A shorter period oscillation is occasionally observed in ultrasmooth films associated with the longer *k* vector spanning the ends of the ''dogbone.'' The periodicity condition is as follows.

Periodicity$=2(k_{BZ}-k_F)$, representing Fermi wave vectors, k_F, spanning the ''belly'' and ''neck'' regions of a spherical Fermi surface distorted at the Brillouin zone boundaries, represented by wave vectors, k_{BZ}. However, it is not at all clear why this particular periodicity should be prevalent, and so similar for different metallic heterostructures.[2] It has been debated whether the spin polarization necessary to couple the magnetic films through the nonmagnetic layer is carried exclusively by the *sp* electrons, and the extent to which the $3d$ states play a role.[7] Local density calculations[8] indicate that the *sp* band contains significant $3d$ character due to hybridization with the $3d$ band for energies close to E_F.

Fermi surface mapping using angle-resolved photoemission has revealed the exchange splitting between the upper and the lower *d* band in Ni,[9] changes in the surface electronic states of hydrogen on W(110),[10] and changes in the spin-orbit splitting of valence states induced at surfaces by adsorbates.[11] Photoemission measurements of the band structure and the Fermi surface are expected to provide insight into the magnetic behavior of $3d$ transition metal alloys. Growth of thin films with molecular-beam epitaxy (MBE) permits us to stabilize materials as thin-film metastable phases, e.g., fcc Co/Cu(100) and fcc Fe/Cu(100).[12,13] It has been demonstrated that it is possible to grow ultrathin fcc $Co_{1-x}Ni_x$ alloy films epitaxially on Cu(100) with variable stoichiometry.[14,15] For $Co_{1-x}Ni_x$ alloy films, the fcc phase is adopted in the whole concentration range and the magnetic moment varies linearly between the values of Ni and Co, while the Curie temperature remains a monotonic function of the composition. The lattice of pseudomorphic fcc Co_xNi_{1-x} alloy films remains constant throughout the whole concentration range. Measurements with the surface magneto-optic Kerr effect (SMOKE) and magnetic dichroism of the Co and Ni $3p$ core levels in photoemission with linearly polarized light (XMLD) have shown that the elemental moments remain constant and finite.

In Sec. III A, we show Fermi surface maps of pure films and alloy films with changing compositions, and compare the fcc bands to the band structure of pure Ni. In Sec. III B, we discuss changes in the dimensions of the Fermi surface and its possible influence on the spanning wave vectors which are thought to be responsible for the GMR oscillations.

II. EXPERIMENT

Angle-resolved photoemission spectroscopy was performed on Beamline 7 at the Advanced Light Source in

Berkeley.[16] The spot size of the light was ~100 μm. The hemispherical electron spectrometer's axis and the photon beam were coplanar. Contour maps of electronic states in momentum space were obtained by fixing the detector's energy window at the Fermi energies and rotating the sample to vary the k vector of the detected states. The energy window at the Fermi energy for all the contour maps was set to 400 meV.

The Cu(100) crystal substrate was mechanically polished and subsequently electropolished before inserting into the vacuum system. A few cycles of Ar^+ sputtering (500 eV) and annealing to 750 K resulted in a sharp $p(1\times1)$ LEED pattern and a contamination-free sample within the sensitivity limit of the XPS spectra using the MgKα source. The growth rate of the Co and Ni sources were controlled by a quartz crystal monitor and the composition was checked with Auger electron spectroscopy (AES) and x-ray photoelectron spectroscopy (XPS), the former being more sensitive to any surface segregation (which was not observed). All the growth conditions have been double checked in a UHV apparatus previously described.[17,18] In this apparatus, the growth rate of the Ni and Co sources were controlled by separate quartz crystal monitors, which were calibrated via high-energy electron diffraction (RHEED) oscillations of Co/Cu(100) and Ni/Cu(100) film growth. The alloy films were carefully grown at 300 K in order to avoid any Cu segregation up from the substrate. The concentration and thickness were monitored *in situ* at the synchrotron with XPS using a standard MgKα source. The quality of the growth was again monitored with low-energy electron diffraction (LEED) and x-ray photoelectron diffraction (XPD). The base pressure in the chamber was smaller than 2×10^{-10} torr and all experiments were performed at room temperature.

III. RESULTS AND DISCUSSION

A. Fermi surfaces of pseudomorphic fcc films on Cu(100)

Co_xNi_{1-x} alloys can be grown as fcc pseudomorphs on a Cu(100) substrate.[14,15] This allowed us to investigate the electronic properties of these alloys with changing composition independent of any change in their lattice structure. All films were grown to a thickness of 8 ML to avoid any contribution from the electronic structure of the Cu substrate. Fixed electron energy contour maps in k space were obtained by fixing the detector's energy window at the Fermi level and rotating the sample. In our experiment, the polar angle was kept constant in the (110) plane. Changing the photon energy in steps of ~5 eV from 75–205 eV, we accessed states located at the Fermi level for the high index planes of the fcc Brillouin zone. Assuming free electron final states, and knowing the angle and energy, the measured intensities can be assigned a definite location in k space.[19]

In Fig. 1, a cross section through extended zone space of the fcc lattice following the procedure outlined by Papaconstantopoulos[8] projected onto the (110) plane, is overlayed onto the measured Fermi surface cut from Cu. The only band that defines the Fermi surface of Cu is the *sp* band, which forms the so-called dogbone structure. The short and long wave vectors thought to be responsible for the exchange coupling in heterostructures are indicated with bold arrows. The dogbone structure referred to above is clearly defined by the *sp* states encompassing a well-defined ''hole'' in the Fermi-energy distribution centered about the x symmetry point.

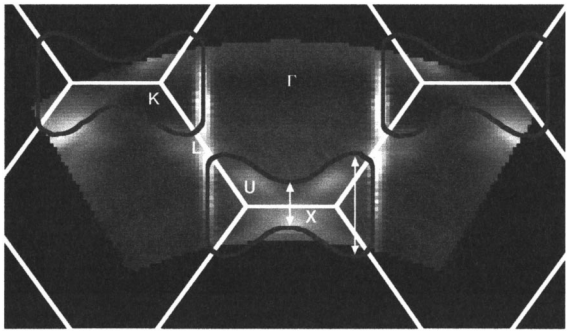

FIG. 1. Calculation of the Cu Fermi surface in the (110) plane using the Slater-Koster (SK) method as an interpolation scheme overlayed on the measured Fermi surface of Cu. We used the SK parameters in the two-center approximation following the procedure outlined by D.A. Papaconstantopoulos (Ref. 8). The bold arrows indicate the short- and long-wave spanning vectors thought to be responsible for the oscillatory exchange coupling in magnetic heterostructures.

Figure 2 displays the calculated Fermi surface cut of the Ni bands, again using the formalism of Papaconstantopoulos.[8] Here we can distinguish between *sp*-minority, *sp*-majority, and *d*-minority states. The dogbone structure remains clearly defined by the *sp*-minority states.

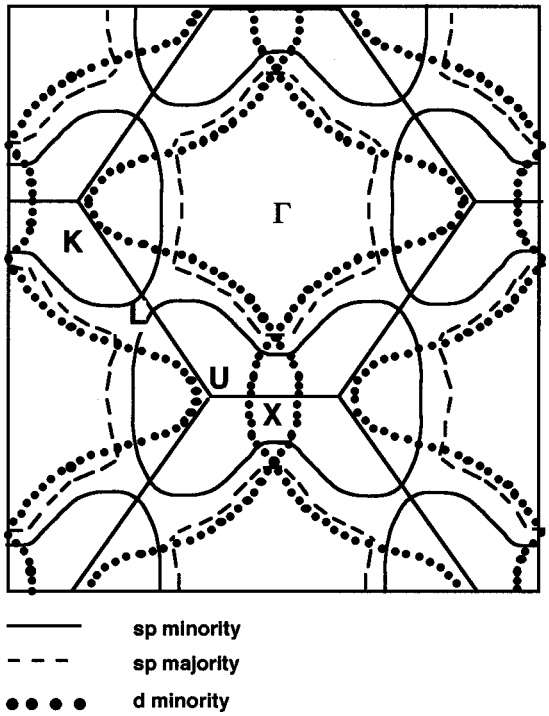

FIG. 2. Calculation of the Ni Fermi surface in the (110) plane using the Slater-Koster (SK) method as an interpolation scheme. We used the SK parameters in the two-center approximation following the procedure outlined by D. A. Papaconstantopoulos (Ref. 8). The horizontal coordinate represents the ⟨110⟩ direction and the perpendicular one the ⟨100⟩ direction. Solid bold lines are the *sp*-minority, dashed lines the *sp*-majority, and dotted lines the *d*-minority bands cutting the Fermi level.

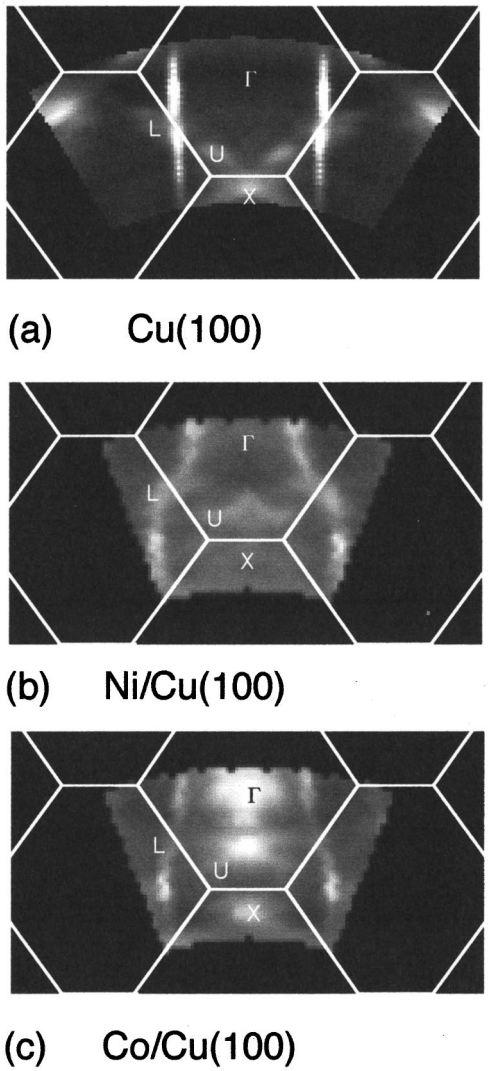

FIG. 3. Photoemission measurements of single crystalline (a) Cu, pseudomorphically grown (b) Ni (8 ML), and (c) Co (8 ML) fcc films. The grayscale images represent the intensity at the Fermi level in the (110) plane in the same geometry as the calculated band structure of Ni in Fig. 2. The energy range is 75–205 eV, and the angle range is $\pm 30°$ for Cu, and $\pm 20°$ for Ni and Co.

Across the belly of the electron hole pockets, the narrow part of the dogbone, we expect, according to our calculation, intensity in the measured Fermi surface from the *sp* states as well as from the *d*-minority states. The *d*-minority band also crosses the *sp*-minority band in the vicinity of the *L* point, as well as following part of the *sp*-majority band on the dogbone location.

We also recorded the Fermi surface of pseudomorphically grown fcc films of Ni and Co on Cu(100) as well as two alloy films of Co_xNi_{1-x} on Cu. States at the Fermi energy were recorded in the high symmetry (110) *k* plane for films 8 ML thick. These fcc films grow nicely on Cu(100) and their crystallographic perfection was confirmed using LEED and XPD.

Figure 3 shows the detailed mapping of these states at the Fermi level in the (110) plane of pure Ni and Co films together with their locations in extended (Brillouin) zone space. An intense bright band connecting the *L* points in the Brillouin zone, observable in all these 3*d* materials, derives from the *sp* band. The dogbone structure about the x point is clearly visible [Fig. 3(a)]. Across the neck of this dogbone feature, we observe the intensity is influenced due to contributions from *d*-bands crossing the Fermi level at this position in *k* space, their number increasing with increasing number of holes in Ni and Co films [Figs. 3(a) and 3(b)]. In particular, the minority-spin *d* band in Ni (Fig. 2) emerges across the neck of this dogbone. With increasing hole concentration in Co [Fig. 3(b)] we see a concentration of intensity in these regions of *k* space, as well as at the Γ point.

The minority and majority spin polarized *d* bands in Ni are not resolved in our measurements. Our photoemission results obtained for pure Ni films are in good agreement with theoretical band-structure calculations (Fig. 2) and the dimensions of the Fermi surface recorded with photoemission are in good agreement with de Haas–van Alphen effect measurements.[20,21]

The experimental maps (Fig. 3) clearly show the effect of increasing hole concentration in the *d* bands of these fcc films, as the Fermi level is lowered when going from Cu to Ni to Co. In addition to an increasing intensity across the neck of the dogbone, we observe increasing intensity contributions at the center of the zone, near the Γ point. Also, we see a change in the size of the these features with increasing hole content. If we now compare the calculated band structures for these 3*d* fcc pseudomorphs (Fig. 4) we see where the *d* bands along this ⟨100⟩ direction cross the Fermi level. From Fig. 4, we see that as the Fermi level shifts to lower energies with increasing hole concentration, it begins to cut through the *d* bands in the center of the zone near the Γ point in the Co pseudomorphs. We can observe this clearly in the Fermi surface maps of Fig. 3: as the number of holes increases, the *d*-hole pocket about Γ increases in size while the Fermi vector at the *sp*-band crossing decreases, which causes the ''holelike'' dogbone dimension to increase.

Figure 5 compares similar plots in the (110) plane of pseudomorphic fcc Co_xNi_{1-x} alloy films on Cu(100). The alloy concentrations are (a) $Co_{35}Ni_{65}$ and (b) $Co_{60}Ni_{40}$. As in the elemental fcc films, in this (110) plane, the dogbone feature due to emission from *sp* states remains characteristic of the whole concentration range. It connects the *L* points in the fcc Brillouin zone more or less continuously throughout momentum space. As the number of holes in the alloy increases, going from pure Ni towards pure Co, emission from new states occurs at the center of the zone as well as across the neck of this dogbone structure. Also with increasing Co concentration, the exchange splitting of the minority and majority *d* bands increases in a way that would indicate that this intensity surrounding the zone center is due mainly to minority spin-polarized *d* states. The dogbone structure, a characteristic feature due to the *sp* band, also collects some *d* character. A marked increase in intensity is observed across the belly of the electron pocket, the midpoints of the dogbone, with increasing number of holes suggesting increasing hybridization with the *sp* band close to the Fermi level. This enhances electron scattering between (mainly minority) *d* and *sp* states in this particular region of *k* space.

Again, we observe a strong contribution due to the *sp* band and a clearly defined dogbone feature. Enhanced intensity in the center of the Brillouin zone and across the midpoints of this dogbone again appears with increased empty-

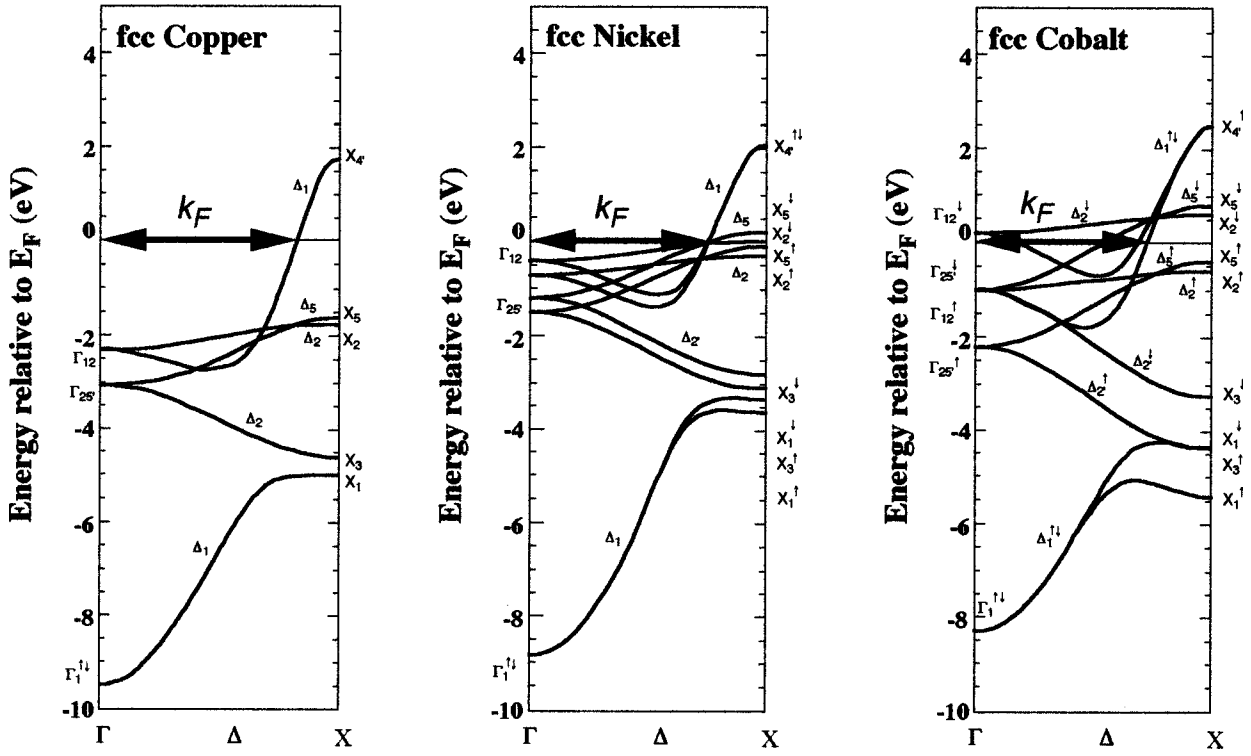

FIG. 4. Band-structure calculation of the fcc $3d$ materials Cu, Ni, and Co along the ΓX direction (Refs. 1 and 27).

ing of the *d* bands. This ''mixing'' of (mainly minority spin) *d* states with *sp* states in specific regions of *k* space creates spin-polarized Fermi surface ''hotspots'' that serve to enhance specific Fermi surface ''nesting'' wave vectors.

Also, the fact that we observe a sharply defined distribution of *sp* states throughout this momentum space is a strong indication that the muffin-tin scattering potentials on the different atomic sites, Ni, Co, are very similar. Any increased diffuseness due to (random) alloying in the patterns appears mainly in the (minority-spin) *d* states, which is due to increased mixing and scattering out of these states at the Fermi level into the *sp* states at these specific regions in *k* space. In Fig. 5, we see a weakening and diffuseness appearing in the emission from the *sp* states connecting the *L* points. This is associated with a (possible) change in chemical composition of the Co-rich CoNi alloys.[22]

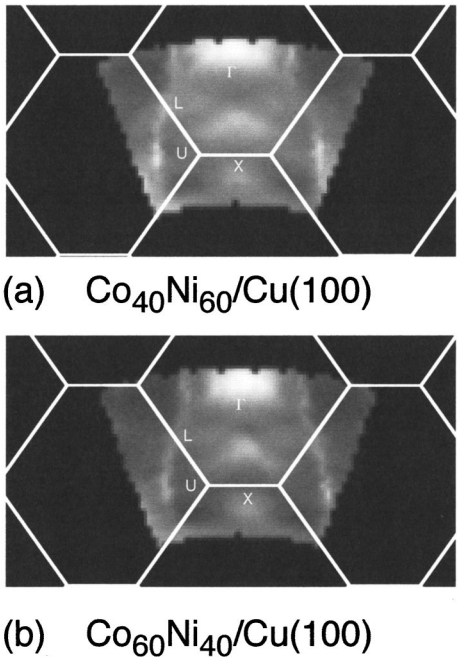

FIG. 5. Photoemission measurements of pseudomorphically grown 8 ML thick fcc Co_xNi_{1-x} films: (a) $Co_{40}Ni_{60}$, and (b) $Co_{60}Ni_{40}$. The grayscale images represent the intensity at the Fermi level in the (110) plane in the same geometry as the calculated band structure of Ni in Fig. 2. The energy range is 75–205 eV, and the angle range is ±30°.

Figure 6 shows Fermi contour maps taken at a photon energy of 190 eV of Cu, 8 ML Ni on Cu(100), and 8 ML Co on Cu(100). At this energy, the measured states are located on a sector of a sphere which corresponds in our angular range with a small deviation to the (100) plane. For Cu, the only feature one can observe is the *sp* band with almost spherical shape. In Ni, the *d*-hole pockets at the x point are clearly visible. For the Co film, the *d*-hole pocket is growing, whereas the *sp*-band feature is decreasing towards the zone center, as we have already observed in the Fermi surface plots in the (110) planes (Figs. 3 and 5).

Figure 7 summarizes the dominant features in our Fermi surface measurements: (i) Enhanced intensity can be observed at the center of the zone with increasing hole concentration due to the minority *d* band cutting the Fermi level in the vicinity of the Γ point. (ii) The *sp* band, forming a dogbonelike structure in all the measured fcc pseudomorphs, can clearly be observed. (iii) At the midpoints of the dogbone, enhanced intensity is observed due to hybridization of the *d* band with the *sp* band. (iv) In the vicinity of the *L* point, we can also observe slight enhancement of intensity (ii). As we can see from Fig. 2, in this region of *k* space, the minority *d* bands also cross the *sp* bands, and the minority *d* band almost coincides with the majority *sp* band in parts of the

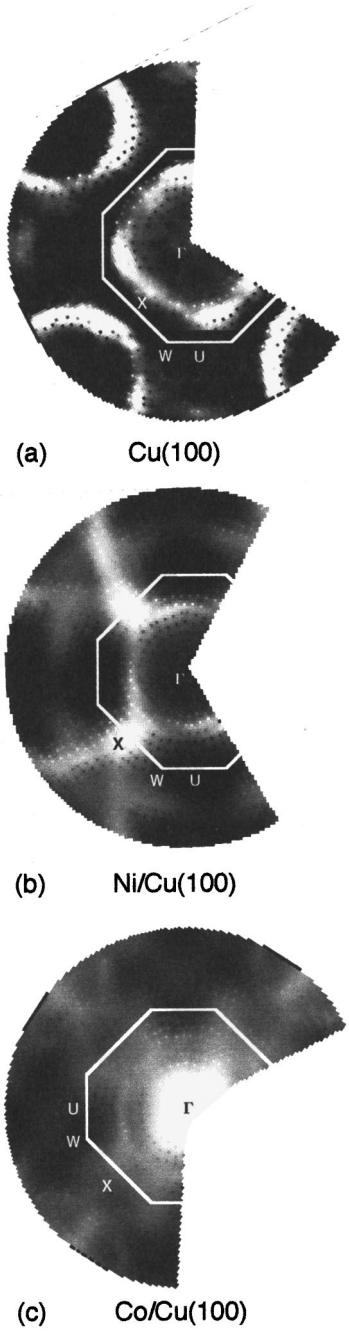

FIG. 6. Fermi contour maps taken at an energy of 190 eV of (a) Cu, 8 ML (b) Ni on Cu(100), and (c) 8 ML Co on Cu(100).

dogbone region, linking the longer spanning wave vector, which would favor the view that minority-spin polarized states foster the GMR coupling mechanism.

B. Neck dimensions and oscillatory coupling

Bruno and Chappert[3] have suggested that the origin of magnetic coupling across a nonmagnetic copper layer is related to the extremal spanning vectors of the dogbone shaped hole Fermi surface formed by the *sp* band. They predict two possible periodicities, around 4.6 and 10.6 Å, due to long and short wave vectors, respectively, spanning favorable nesting regions of this dogbone Fermi surface feature in copper. The exact relationship between the expected wavelength

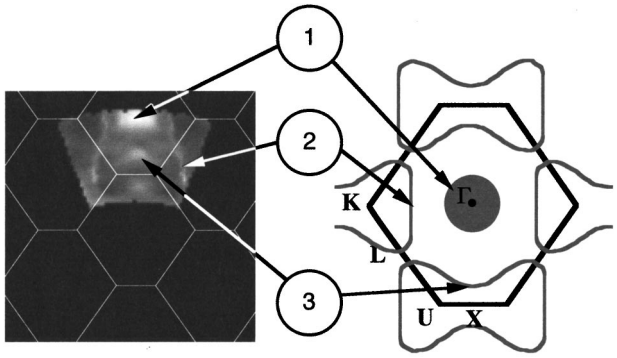

FIG. 7. Dominant features in the Fermi surface map of $Co_{60}Ni_{40}$ on Cu(100): (1) Enhanced intensity can be observed at the center of the zone with increasing hole concentration due to the minority *d* band cutting the Fermi level in the vicinity of the Γ point. (2) The *sp* band, forming a ''dogbone''-like structure in all the measured fcc pseudomorphs, can clearly be observed. (3) At the midpoints of the ''dogbone,'' enhanced intensity is observed due to hybridization of the *d* band with the *sp* band.

for these oscillations and the wave vector along the ⟨100⟩ direction, is $k_{osc}=2(k_{BZ}-k_F)$: In Fig. 4, k_F is indicated as a bold arrow. For increasing hole concentration, Cu→Ni→Co, one expects that k_{osc} increases slightly due to the Fermi level crossing of the *sp* band occurring at smaller k_F values, which increases the size of the wave vector spanning the dogbone hole pocket (Fig. 4).

From our measurements, we can assign the wave vectors for the long oscillation period. These values span the range of long periodicities usually observed.[2] The trend in the Co_xNi_{1-x} alloys is that for increasing Co content, the appropriate spanning wave vector dimension of the dogbone is increasing so that the associated oscillation period should decrease. The resolution of our measurements does not allow a more precise prediction of this period. However, as indicated in Fig. 4, a strong hybridization of (mainly minority) *d* with *sp* states is expected to occur at these extremal points of the dogbone, thus giving a strong contribution to hybridization and spin polarization of the *sp* band. At the other extremal point of the dogbone Fermi surface, at the necking region of the electron pocket, shorter periodicity oscillations (i.e., longer spanning wave vectors) are predicted and have been observed in smooth films.[23] We note that our measurements show only small intensity enhancement from the *d* bands or ''hot spot'' formation in this region of *k* space. Yet, it is not clear from our measurement to what extent the *sp* band gets polarized in this region, and therefore we cannot make a definite statement concerning these shorter periodicity coupling oscillations. One can still ask the question: Since these *sp* states do not appear to be as strongly mixed with *d* states as those at the belly region, what else could be the reason for the shorter periodicity coupling oscillations giving rise to the spin polarization?

A recent paper addresses the problem of spin-relaxation of the conduction electrons[24] and predicts that at certain hot spots on the Fermi surface, defined to be near a zone boundary, the spin in some metals decays unexpectedly fast. This serves to spin polarize the *sp* bands in an otherwise nonmagnetic intermediate layer. The necking of the Fermi sphere at a zone boundary of the fcc Brillouin zone creates such a

scattering hot spot and determines the long extremal wave vector of the dogbone hole pocket in the fcc Fermi surface. We also note that the *sp* band is, more or less, continuous throughout this *k* space, connecting *L* points and particularly the dogbone feature, which defines these spanning wave vectors. Strong hybridization and interactions between *sp* and spin-polarized *d* states spanning the dogbone minimum at the belly Fermi wave vector, spin polarize the *sp* states by scattering throughout this momentum space. A recent high-resolution photoemission measurement of these *sp* states[25] shows the exchange splitting to be of the order of 0.27 eV throughout momentum space. Also, the spectral broadening of the minority-spin states are significantly larger than that of the majority-spin states, indicative of shorter lifetimes due to stronger scattering out of these states and a stronger polarizing interaction between minority-spin *d* and *sp* states. The *sp* states are thus spin polarized uniformly throughout *k* space, with nesting wave vectors favoring particular ''long'' and ''short'' period spin-polarized oscillations, as has been suggested from theoretical considerations.[3,26]

IV. SUMMARY

In summary, we have mapped states in momentum space at the Fermi energy using a range of photon energies in angle-resolved photoemission, for a series of magnetic transition metals as well as for their binary alloys as a function of stoichiometry. These alloys possess the same crystallographic structure as that of the Cu(100) substrate when grown as ultrathin epitaxial layers. This implies that the position of the Fermi level is a direct reflection of the hole concentration in the *d* bands, which we can vary by either changing the elemental material or by alloying the various elements. This is why we expect the Fermi surface maps in *k* space to evolve gradually with alloy stoichiometry.

As a result, we see sharply defined *sp* states throughout *k* space characterized by the same dogbone Fermi surface hole structure characteristic the ⟨110⟩ projection of fcc copper. Emptying the *d* bands leads to states appearing localized in the dogbone region and as a diffuse region about the zone center. Mixing of *d* and *sp* states, mainly of minority spin polarization, in regions of *k* space identified previously with the locations of spanning wave vectors, are driving minority-spin RKKY Fermi surface oscillations, which couple magnetic layers separated by nonmagnetic fcc spacer films in spin-valve heterostructures showing GMR oscillations. The observation of a similar shaped *sp* feature in all these fcc pseudomorphs could explain why the long-wavelength oscillations are similar in all the fcc heterostructures.

Another question that needs to be addressed is to what extent does the random substitution of the elements on a fixed fcc lattice significantly broaden the electronic states in energy and *k* space? The present results suggest that the angular distributions observed are relatively insensitive to the alloying and changing stoichiometry. Any diffuseness in the patterns appears to be masked by the usual photoemission lifetime broadening effects. Some increasing diffuseness is observed in the alloys, which could arise from random scattering effects in the potential, but these effects appear to be second order compared with similar lifetime broadening observed in the pure elemental films and single crystal copper. The photoemission Fermi surface dimensions of elemental Ni pseudomorphic layers are in close agreement with other experimental determinations of the Fermi surface parameters of bulk Ni,[20,21] and first principle calculations of the Ni Fermi surface.[27] The diffuseness is more apparent, in general, within the *d*-states distribution rather than the more free-particle *sp*-states distribution.

The present photoemission results show that the *sp* band is the dominating feature of the Fermi surface of these fcc pseudomorphs forming a dogbone shaped hole pocket characteristic of the Cu(110) plane. We observe an enhancement of intensity across the belly region of the dogbone, which originates from the hybridization of the *d* band with the *sp* band, and polarizes this band in a region of *k* space, which is important for the magnetic coupling underpinning the GMR effect.

ACKNOWLEDGMENTS

This work was funded by a grant from the Department of Energy, Office of Basic Energy Science, Grant No. R-5-32633, A02. The Advanced Light Source is supported by the Director, Office of Science, Office of Basic Energy Science, Material Science Division, of the U.S. Department of Energy under Contract No. DE-AC03-76SFF00098 at Lawrence Berkeley National Laboratory.

[1] F. J. Himpsel, J. E. Ortega, G. J. Mankey, and R. F. Willis, Adv. Phys. **47**, 511 (1998), and references therein.
[2] S. S. P. Parkin, Phys. Rev. Lett. **67**, 3598 (1991).
[3] P. Bruno and C. Chappert, Phys. Rev. Lett. **67**, 1602 (1991).
[4] P. Bruno, Phys. Rev. B **52**, 411 (1995).
[5] M. D. Stiles, Phys. Rev. B **48**, 7238 (1993).
[6] M. T. Johnson, S. T. Purcell, N. W. E. McGee, R. Cochoorn, J. aan de Stegge, and W. Hoving, Phys. Rev. Lett. **68**, 2688 (1992).
[7] D. M. Edwards, J. Mathon, R. B. Muniz, and M. S. Phan, Phys. Rev. Lett. **67**, 493 (1991).
[8] D. A. Papaconstantopoulos, *Handbook of the Band structure of Elemental Solids* (Plenum Press, New York, 1985).
[9] T. Greber, T. J. Kreutz, and J. Osterwalder, Phys. Rev. Lett. **79**, 4465 (1997).
[10] E. Rotenberg and S. D. Kevan, Phys. Rev. Lett. **80**, 2905 (1998).
[11] Eli Rotenberg, J. W. Chung, and S. D. Kevan, Phys. Rev. Lett. **82**, 4066 (1999).
[12] J. R. Cerda, P. L. de Andres, A. Cebollada, R. Miranda, E. Navas, P. Schuster, C. M. Schneider, and J. Kirschner, J. Phys.: Condens. Matter **5**, 2055 (1993).
[13] S. Müller, P. Bayer, C. Reischl, K. Heinz, B. Feldmann, H. Zillgen, and M. Wuttig, Phys. Rev. Lett. **74**, 765 (1995).
[14] F. O. Schumann, S. Z. Wu, G. J. Mankey, and R. F. Willis, Phys. Rev. B **56**, 2668 (1997).
[15] F. O. Schumann, R. F. Willis, K. G. Goodman, and J. G. Tobin, Phys. Rev. Lett. **79**, 5166 (1997).

[16] A. Warwick, P. Heimann, D. Mossessian, W. McKinney, and H. Padmore, Rev. Sci. Instrum. **66**, 2037 (1995).
[17] F. Huang, M. T. Kief, G. J. Mankey, and R. F. Willis, Phys. Rev. B **49**, 3962 (1994).
[18] G. J. Mankey, M. T. Kief, and R. F. Willis, J. Vac. Sci. Technol. A **9**, 1595 (1991).
[19] E. W. Plummer and W. Eberhardt, Adv. Chem. Phys. **49**, 533 (1982).
[20] D. C. Tsui, Phys. Rev. **164**, 669 (1967).
[21] A. V. Gold, J. Low Temp. Phys. **16**, 3 (1974).
[22] J. L. Robertson, G. E. Ice, C. J. Sparks, X. Jiang, P. Zschack, F. Bley, S. Lefebvre, and M. Bessière, Phys. Rev. Lett. **82**, 2911 (1999).
[23] P. Segovia, E. G. Michel, and J. Ortega, Phys. Rev. Lett. **77**, 3455 (1996).
[24] J. Fabian and S. Das Sarma, Phys. Rev. Lett. **81**, 5624 (1998).
[25] D. Y. Petrovykh, K. N. Altmann, H. Hoechst, M. Laubscher, S. Maat, G. J. Mankey, and F. J. Himpsel, Appl. Phys. Lett. **73**, 3459 (1998).
[26] F. Bruno and C. Chappert, Phys. Rev. B **46**, 261 (1992).
[27] C. S. Wang and J. Callaway, Phys. Rev. B **15**, 298 (1977).